Nanoscale

PAPER

View Article Online
View Journal | View Issue

Cite this: *Nanoscale*, 2018, **10**, 3037

An underwater superoleophobic nanofibrous cellulosic membrane for oil/water separation with high separation flux and high chemical stability†

Seong Kyung Hong,[a] Seonghan Bae,[a] Hyungkook Jeon,[a] Minseo Kim,[a] Seong J. Cho *[b] and Geunbae Lim *[a]

Received 3rd November 2017,
Accepted 31st December 2017

DOI: 10.1039/c7nr08199e

rsc.li/nanoscale

Oil spills and an increasing demand for the treatment of industrial oily wastewater are driving the need for continuous large-scale oil/water separation processes. Herein, we report a nanofibrous cellulosic membrane (NFC membrane) for the continuous high-flux separation of large amounts of oil/water mixtures. The NFC membrane was fabricated using wet electrospinning, a facile yet effective method for stacking nanofibrous membranes with uniform porous structures on a substrate. Owing to its cellulosic nature, the membrane showed excellent underwater superoleophobicity along with robust chemical stability and was able to separate oil/water mixtures at efficiencies exceeding 99%. Repetitive oil/water separations could be performed using a single membrane, during which the oil content in the filtrate remained extremely low (<29 ppm). The nanofibrous membrane exhibited a fine porous structure that was interconnected throughout the membrane, resulting in a high oil intrusion pressure (>30 kPa) that allowed not only gravity-driven but also pressure-driven separation of oil/water mixtures. The separation flux reached 120 000 L m^{-2} h^{-1} during pressure-driven separations, which is a very promising feature for actual applications such as the large-scale treatment of industrial oily wastewater.

1. Introduction

Frequent oil spills and an increasing need to treat industrial oily wastewater have heightened interest in oil/water separation for environmental, economic, and social issues.[1–3] The removal of oil from large amounts of oily water is essential to mitigate adverse environmental events upon discharge or reuse. Consequently, there is an increased demand for the development of effective and inexpensive approaches to remediate large volumes of oil/water mixtures. Because oil and water are incompatible, separation occurs at the interfacial level according to the specific wetting behavior of the separation membrane. Separation methods leveraging special wetting phenomena that enable simultaneous wetting by oil and water are of particular interest because they effectively remove oil from water without an external energy input.

There are numerous membrane designs for effective separation, which can be categorized into two types: the superhydrophobic design and the superoleophobic design. The more traditional approach uses a superhydrophobic/superoleophilic membrane.[4–8] Inspired by the superhydrophobic surface of a lotus leaf, these membranes possess two key characteristics: a hierarchically rough surface and a chemically modified surface having a low surface energy.[6,9–19] Unfortunately, the commonly used low-energy materials require special equipment and complex processes for their manufacture and are harmful to the environment and human health. Furthermore, because water typically has a higher density than oil, it naturally forms a barrier between the oil and the membrane, thereby preventing the permeation of the oil through the membrane. Importantly, these superoleophilic material membranes are easily fouled, blocked, and even damaged by the oil that has permeated into the membrane during the separation process. This fouling results in a gradually decreased oil/water separation efficiency and limits practical applications.[10,20]

Recently developed membranes having underwater superoleophobicity are of particular interest for oil/water separation because the oil phase is repelled while the water phase easily

[a]*Department of Mechanical Engineering, Pohang University of Science and Technology (POSTECH), 77 Cheongam-Ro, Nam-Gu, Pohang 790-784, the Republic of Korea. E-mail: limmems@postech.ac.kr; Fax: +82-54-279-0479; Tel: +82-54-279-2186*
[b]*School of Mechanical Engineering, Chungnam National University (CNU), 99 Daehak-Ro, Yuseong-Gu, Daejeon 305-764, the Republic of Korea. E-mail: scho@cnu.ac.kr; Tel: +82-42-821-5648*

†Electronic supplementary information (ESI) available. See DOI: 10.1039/c7nr08199e

penetrates the membrane.[21–23] Such membranes, when immersed in water, repel oil while permitting water to pass through, and enable a high oil/water separation efficiency that can be driven only by gravity. Their resistance to fouling from oil permits underwater superoleophobic membranes to be used repetitively and handle large amounts of oil/water mixtures. The underwater superoleophobicity of such membranes is conferred by various materials, including hydrogels,[24,25] silica,[26] palygorskite,[27] TiO_2,[28,29] ZnO,[30,31] $CaCO_3$,[32] $Cu(OH)_2$,[33,34] zeolites,[35] and graphene oxide.[36,37] Because water has a greater density than most oils, the water layer is constantly found beneath the oil layer and in direct contact with the membrane. This type of water-removal membrane allows the continuous separation of oil/water mixtures by using gravity alone. Continuous high-volume separation is essential for the treatment of industrial oily wastewater and after oil spills.

Although an underwater superoleophobic membrane is suitable for continuous separation, it should ideally have two additional factors to process large amounts of oil/water mixtures efficiently: high separation flux and high oil intrusion pressure. A high separation flux enables the separation membrane to process large volumes quickly. A high oil intrusion pressure provides a high separation capacity. Throughout the separation, oil accumulates and forms an oily layer that applies a constant pressure onto the membrane. To achieve complete separation of the oil from the water, the membrane must prevent the oil from penetrating under the constant pressure. As the separation continues, the height of the oil column increases, thereby increasing the pressure on the membrane, which eventually causes the oil to penetrate the membrane when it reaches the oil intrusion pressure of the membrane. For the separation to continue, the oil must be drained off before the oil column reaches this critical height. Therefore, the higher the oil intrusion pressure, the larger the amount of oil/water mixture that can be processed without stopping.

However, in this context, there is an engineering issue of concern. The two factors (high separation flux and oil intrusion pressure) act in opposition, such that a membrane having a high separation flux usually has a low oil intrusion pressure, and *vice versa*. The flux discussed here specifically refers to the gravity-driven separation flux without any external pressure applied during the process. Of the two factors, having a high oil intrusion pressure is favored against having a high separation flux, as the flux of the membrane with high oil intrusion pressure can be enhanced by applying external pressure during oil/water separation. Reported underwater superoleophobic membranes usually exhibit high gravity-driven separation fluxes ranging from *ca.* 50 000 to over 100 000 L m^{-2} h^{-1}.[32,35,38,39] However, oil intrusion pressures have not been reported in most cases. Furthermore, even for the handful of studies that did measure the oil intrusion pressure, the membranes exhibited underwhelming results: oil intrusion pressures ranging from sub-1 to 6.1 kPa.[27–29,35,38,39] A uniform, fine porous structure throughout the membrane is essential to provide it with a high oil intrusion pressure. Concurrently, the porous structure must be interconnected to provide a high separation flux and thus be viable for large-scale oil/water separation.

Additionally, during the continuous separation process, the water phase always remains in contact with the membrane. A chemically harsh aqueous environment can damage the exposed membrane during continuous oil/water separation. Previous studies on underwater superoleophobic membranes mainly examined polymer-coated membranes, which suffer from high material costs and complex manufacturing processes. They often cannot survive the harsh conditions of a prolonged separation process. Thus, the stability of a membrane in harsh chemical environments such as strongly acidic, alkaline, or saline conditions is important for practical applications.

We report herein a nanofibrous cellulosic membrane (NFC membrane) that has the beneficial features of high oil intrusion pressure and high chemical stability. This membrane was fabricated using wet electrospinning, which is a facile yet effective method for stacking nanofibrous membranes having uniform porous structures on a substrate. The cellulosic nanofibrous composition had an interconnected fine porous structure and displayed excellent underwater superoleophobicity [underwater oil contact angle (OCA) of >150°] with a high oil/water separation efficiency (>99%), high separation flux (120 000 L m^{-2} h^{-1}), and high oil intrusion pressure (>30 kPa). The membrane could be used repetitively for multiple oil/water separations, during which the oil content in the filtrate remained extremely low (<29 ppm). Cellulose, the base material of the NFC membrane, is one of the most abundant natural polymers. It has excellent chemical resistance and provided the membrane with stable superoleophobicity even in chemically harsh environments such as strongly acidic, alkaline, or saline conditions. The membrane could process oil/water mixtures in these harsh environments at separation efficiencies exceeding 99%.

2. Experimental section

2.1. Materials

Cellulose acetate (CA) (M_n 70 000) was purchased from Sigma–Aldrich (USA), and dimethylacetamide (DMAc) and acetone were purchased from Samchun Pure Chemical (KR). All chemicals were used as-received without further purification.

2.2. Wet electrospinning of the cellulose acetate membrane

A schematic representation of the fabrication steps used to prepare the membrane is given in Fig. 1a. A mixture of acetone and DMAc at a volume ratio of 2 : 1 was used to dissolve CA to a concentration of 17 wt%. The solution was stirred overnight (12 h) to ensure complete and homogeneous dissolution. A fabrication system consisting of a cylindrically shaped bath (height and diameter of the bath were 15 and 150 mm, respectively), a high-voltage source, and a syringe pump was assembled to conduct the wet electrospinning. The bath was

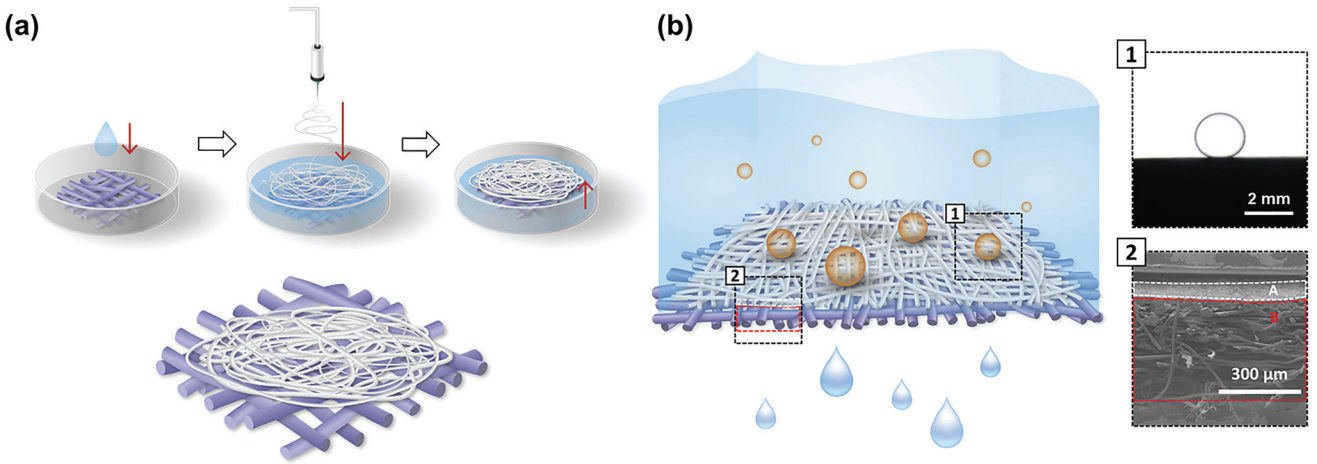

Fig. 1 (a) Fabrication process of the NFC membrane: deposition of the electrospun cellulose acetate (CA) membrane on clean paper. (b) Schematic diagram of an oil/water separation with the underwater superoleophobic NFC membrane [inset 1: underwater oil contact angle (OCA); inset 2: cross-sectional scanning electron microscope (SEM) image of the NFC membrane].

electrically grounded with external wiring. The bath was filled with a conductive liquid (150 mL of 1 M NaCl aqueous solution); the surface of the liquid acted as the collector. A sheet of clean paper was immersed beforehand in the bath, and then the CA nanofibrous membrane was electrospun onto the surface of the liquid. The electrospinning process was performed at a high voltage of 19 kV at a 10 cm distance. The formed CA nanofibrous membrane, floating on the liquid surface, was then stacked on top of the immersed clean paper by scooping the CA nanofibrous membrane out of the bath. The collected membrane was rinsed in running deionized (DI) water to remove any residual conductive liquid and then dried in a desiccator overnight. All electrospinning experiments were conducted at room temperature and low humidity (relative humidity of 20%). The fabrication process used here is different from the conventional electrospinning method where a flat metal collector (a sheet of aluminum foil) is normally used. This is because the CA nanofibrous membrane collected on an aluminum foil collector could not be detached without being damaged or even torn.

2.3. Underwater oil contact angle measurement

The surface-wetting properties of the membranes were studied by underwater OCA measurements. Oil droplets with a volume of 5.0 μL were carefully placed on the membrane, which was then placed underwater. An obtained image was then processed using the ImageJ software to outline the underwater OCAs for the different oils on the NFC membrane.

2.4. Oil/water separation experiments

The NFC membrane (pre-wetted by water) with a radius of 17 mm was fixed underneath a conical tube with both sides cut off. Various mixtures of water and oil (*n*-hexane, mineral oil, petroleum ether, or kerosene) were poured into the tube. The entire separation process was solely driven by gravity. Oil/water mixtures and oil-in-water emulsions were prepared for separation efficiency determination. A mixture was stirred with water for 30 min. The resulting mixture was treated with an ultrasonic generator (40 kHz, 150 W) for 30 min. The separation efficiency was calculated in terms of the oil rejection ratio. The oil content in the permeate was calculated using the transmittance of the feed emulsion and permeate.

2.5. Determining the pore size distribution of the membrane

Porosimetry was used to determine the pore size distribution of the membrane. Porosimetry is an analytical technique used to determine various quantifiable aspects of a material's porous nature, such as pore size distribution. The technique involves the intrusion of a non-wetting liquid (often mercury) at a high pressure into a material through the use of a porosimeter. The pore size can be determined based on the external pressure needed to force the liquid into a pore against the opposing force of the liquid's surface tension. The biggest pores of the membrane are penetrated first as they are the easiest for the non-wetting liquid to penetrate through. This is followed by the penetration of smaller pores of the membrane and in a cumulative sense, the pore size distribution of the membrane is obtained.

2.6. Instruments and measurements

The surface morphologies of the membranes were examined by scanning electron microscopy (SEM; Mini SEM). Oil droplets with a volume of 5.0 μL were placed carefully on the membrane, which was then placed underwater. An obtained image was then processed using the ImageJ software to outline the underwater OCA of each oil droplet on the NFC membrane. The oil/water separation efficiency was determined by UV-visible spectroscopy. The porosimetry was handled by a porosimeter (CFP 1200AE, PMI, USA).

3. Results and discussion

3.1. NFC membrane morphology

The NFC membrane was prepared by electrospinning a CA nanofibrous membrane onto a sheet of clean paper immersed in water. The as-prepared membrane was rinsed in running DI water to remove any residual conductive liquid and then dried in a desiccator overnight. Fig. 1b depicts the NFC membrane showing the underwater superoleophobicity, a unique wetting property that strongly repels oil underwater. This special wetting property derives from the inherent hydrophilicity of both layers that comprise the NFC membrane: the CA nanofibrous membrane and the clean paper. The NFC membrane repelled oil when immersed underwater (inset 1) where the NFC membrane formed a contact angle greater than 150° with the oil droplet.

As previously noted in the fabrication details, the NFC membrane had a two-layered structure. Inset 2 of Fig. 1b is a cross-sectional SEM image of the NFC membrane, where layers A and B represent the CA nanofibrous membrane and the clean paper, respectively. Each layer plays a significant role during the oil/water separation process. Since both layers are based on cellulosic polymers, they are inherently hydrophilic and have good chemical stability, which is beneficial to oil/water separation in chemically harsh environments. Notably, the CA nanofibrous membrane features micro-sized pores that block oil droplets during the oil/water separation. In addition, the fine pore size grants the whole membrane a high oil intrusion pressure, which allows oil/water separation even under high-pressure conditions. The clean paper acts as a mechanical reinforcement layer while being a thick reservoir for water, thereby keeping the entire NFC membrane wet during the oil/water separation process.

Fig. 2a is a top-view SEM image that shows the surface morphology of the NFC membrane. The top layer consists of CA nanofibers with varying diameters ranging from 100 to 700 nm, with an average of 450 nm. The pore size distribution of the membrane is shown in Fig. 2b. The pore diameter ranges from sub-1 to 5 μm, with an average pore diameter of 2.2 μm. The nanofibrous nature of the membrane naturally forms a fine porous structure, interconnected throughout the membrane. These traits conferred a high oil/water separation flux as well as a high oil intrusion pressure on the NFC membrane.

3.2. Wetting characteristics of the NFC membrane

The underwater oil wettability of the membrane was evaluated by immersing it upside-down in water, then placing an oil droplet underneath the membrane. In the water/oil/membrane three-phase system, the NFC membrane could not be wetted by oil underwater, with the oil droplet forming a contact angle higher than 150°. The water trapped between the oil droplet and the membrane surface made the membrane superoleophobic underwater. Additionally, the NFC membrane exhibited underwater superoleophobicity toward various types of oils (*i.e.*, mineral oil, kerosene, *n*-hexane, and petroleum ether). Fig. 3 shows the contact angles of the various oil droplets on the NFC membrane underwater; optical images of these oil droplets are also shown in the insets at the top of each corresponding bar. Without an exception, all of the oil droplets formed a contact angle greater than 150° on the membrane,

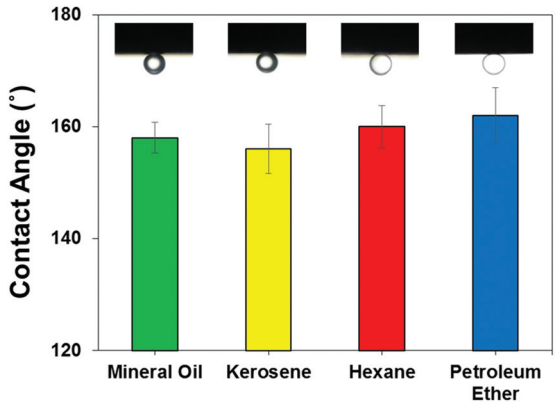

Fig. 3 Underwater oil contact angles (OCAs) of various oils on the NFC membrane.

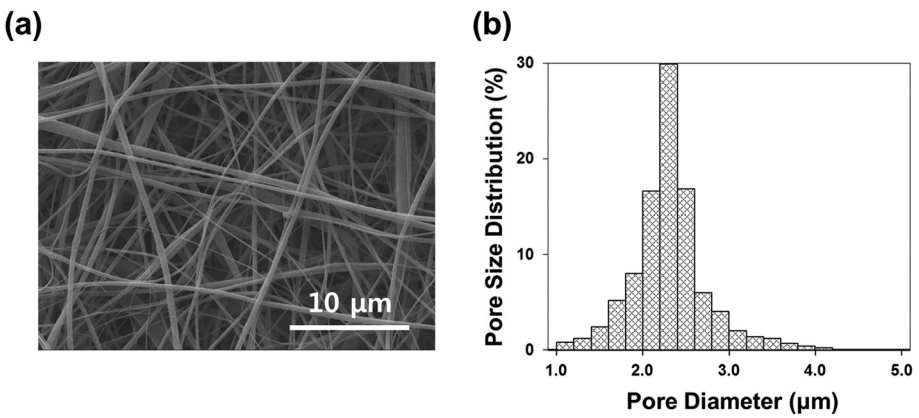

Fig. 2 (a) Scanning electron microscopy (SEM) image of the surface of the NFC membrane. (b) Pore size distribution of the NFC membrane.

confirming the membrane's underwater superoleophobic properties and its potential for oil/water separation applications.

3.3. Oil/water separation

Having demonstrated the underwater superoleophobic characteristics, the NFC membrane was then tested for its oil/water separation capability. Fig. 4a shows the experimental set-up of the oil/water separation process. The NFC membrane was fixed onto one end of the cylindrical tube while an oil/water mixture was poured into the other end. The mixture consisted of 20 mL of DI water and 20 mL of mineral oil. The membrane needed to be wetted by a stream of water prior to the separation to trigger the underwater superoleophobic characteristics. To emphasize the separation process visually, DI water was dyed with methylene blue and mineral oil was dyed with Oil Red O for color contrast. Relying solely on gravity, water permeated through the membrane and collected in the glass beaker below, while mineral oil remained above the membrane because of the underwater superoleophobicity. The whole separation process was accomplished within a few seconds. Various types of oil (*i.e.*, mineral oil, kerosene, *n*-hexane, and petroleum ether) were tested for oil/water separation and the correlating separation efficiency was calculated using eqn (1).

$$E_{ff} = \left(1 - \frac{C_p}{C_o}\right) \times 100\% \quad (1)$$

where C_p and C_o are the amounts of oil in the original oil/water mixture and the filtered mixture, respectively. Fig. 4b shows that the NFC membrane exhibited separation efficiencies exceeding 99% for all of the oils tested, indicating its general suitability for oil/water separations.

3.4. Oil/water separation in chemically harsh environments

The NFC membrane is based on cellulosic polymers that provide inherent hydrophilicity and chemical stability. These features greatly enhance the membrane's applicability in chemically harsh environments compared with other materials such as hydrogels, inorganic metal oxides, and polymer composites. The oil/water separation environment is often chemically harsh, for example, strongly saline, acidic, or alkaline. Therefore, it was crucial to establish whether the oil/water separation efficiency of the NFC membrane could be sustained in such environments.

The superoleophobic stability was first tested by measuring the contact angle of oil droplets on the NFC membrane in saline (1 M NaCl), acidic (1 M HCl), and alkaline (1 M NaOH) environments. Here, mineral oil was used for the contact angle measurement. Fig. 5a shows that the contact angle of the oil droplet remained above 150° in all of the chemically harsh environments tested, which indicated the stable underwater superoleophobicity of the membrane even in saline, acidic, or alkaline environments.

Oil/water separation tests were also carried out in these specific environments, also with mineral oil. Fig. 5b shows the oil/water separation efficiency of the NFC membrane in saline, acidic, and alkaline environments. The separation efficiency remained well above 99% for all of the environments tested, which further confirmed its applicability for oil/water separation in chemically harsh environments.

3.5. Repetitive oil/water separations

For the NFC membrane to be practical for oil/water separation, the membrane should be able to withstand repetitive separations of oil/water mixtures. The underwater superoleophobic membranes were resistant to oil fouling and generally showed great reusability in the oil/water separation process. The membrane detailed herein not only showed excellent reusability, but the oil concentration of the filtered mixture remained below 29 ppm throughout repetitive oil/water separations. (The U.S. Environmental Protection Agency regulates a maximum oil concentration of 29 ppm in discharged water.[40]) Fig. 6 shows the oil concentration of the filtered mixture for multiple cycles of oil/water separation tests, separating 2 L of an oil/water mixture (50 : 50 DI water and mineral oil) per cycle accumulating to 10 L. The average density of the oil/water mixture (mineral oil/water) used here is 0.9 kg m^{-3}. During each cycle, the inflow of the mixture was controlled manually so that 1 L of the mixture would be constantly remaining in the separation device. At the end of each cycle, 1 L of oil would be remaining inside the separation device, while 1 L of pure

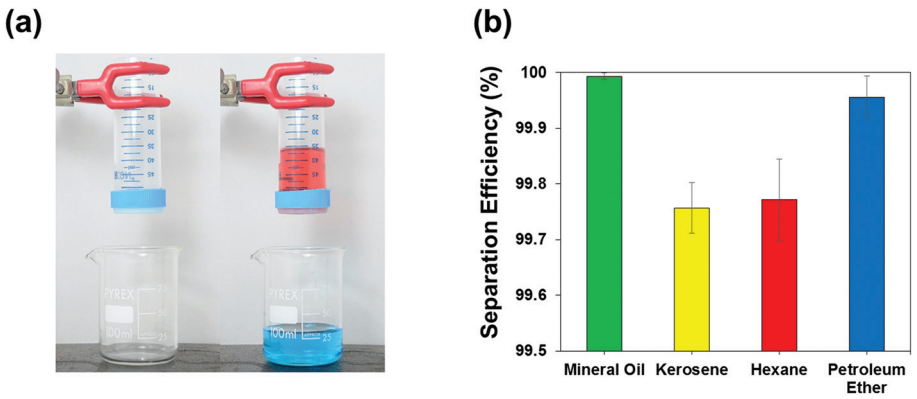

Fig. 4 (a) Experimental set-up of the oil/water separation process. (b) Separation efficiency of various oils using the NFC membrane.

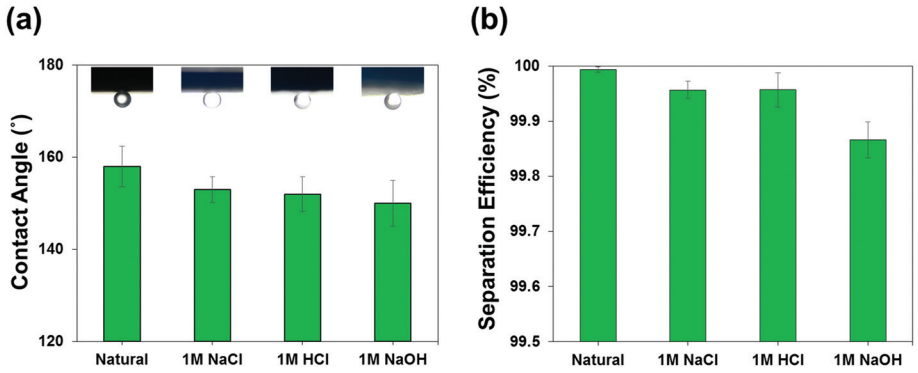

Fig. 5 (a) Underwater oil contact angles (OCAs) of mineral oil on the NFC membrane in various chemically harsh environments. (b) Separation efficiency of mineral oil in chemically harsh environments.

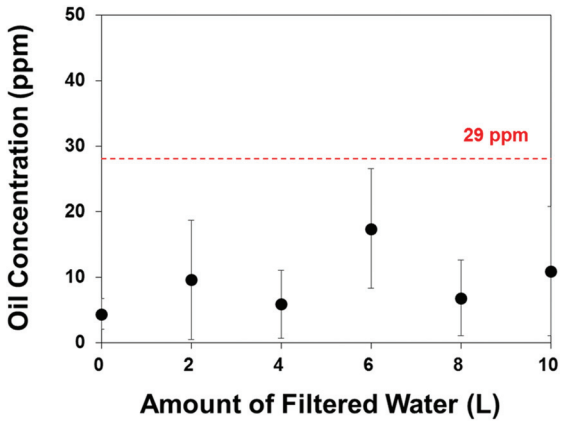

Fig. 6 Repetitive oil/water separations using the NFC membrane. The red dotted line at 29 ppm indicates the maximum oil concentration regulated by the U.S. Environmental Protection Agency.

water would be in the filtrate beaker. The constant pressure applied on the NFC membrane from the stacked mixture is around 1.3 kPa to 1.5 kPa. After a single cycle had been completed, the separation device was immediately drained out of the filtered oil and poured with a fresh oil/water mixture for the next cycle. The time interval between each cycle was less than 10 seconds. The results show that the oil concentration remained below 29 ppm for all of the separation cycles, proving that the NFC membrane can effectively separate more than 10 L of the oil/water mixture. The entire separation was handled by a small membrane with an effective surface area of 6.1 cm^2 (Fig. 4a). Considering that the separation membrane can be easily scaled up to a larger size, there is clearly great potential for industrial-scale oil/water separation applications. The same repetitive oil/water separation experiment was carried out for only the clean paper without the CA nanofibrous membrane stacked on top. The results are shown in Fig. S2 of the ESI.† The clean paper failed to keep the oil concentration in the filtrate lower than 29 ppm and was completely unusable as an oil filter after the first cycle of the separation process as the oil concentration in the filtrate exceeded over 3000 ppm.

3.6. Oil intrusion pressure of the NFC membrane and its robustness under high-pressure separation conditions

The oil intrusion pressure was measured for further study of the oil/water separation ability of the NFC membrane. This property is the maximum pressure that the membrane can withstand without letting the oil penetrate through. This is a crucial performance factor when evaluating oil/water separation membranes, since it is directly proportional to the amount of oil/water mixture the membrane can process without draining out the residual oil layer. Membranes with high oil intrusion pressures are better for larger-scale applications because of their superior resistance to high-pressure environments. During oil/water separation, membranes with low oil intrusion pressures quickly reach their limits and thus are not ideal for large-scale separation applications or for high-pressure environment separations.

The NFC membrane described in this work, on the other hand, exhibited a high oil intrusion pressure due to its fine pore size derived from the intrinsic nanofibrous structure. We conducted experiments using NFC membranes of five different thicknesses of the electrospun CA layer (40, 80, 120, 160, and 200 μm). Normally, the oil intrusion pressure is measured by the height of the stacked oil column during the separation process. However, the pressure generated from the stacked oil was insufficient for our membrane to reach its oil intrusion pressure. A pressure pump was thus used to apply additional pressure on the oil column manually. The bottom surface of the NFC membrane was continuously monitored *via* video recording while gradually increasing the applied pressure. The pressure was measured up to the point when an oil droplet passed through and formed on the bottom surface of the membrane. The oil intrusion pressures of the five membranes are shown as the experimental oil intrusion pressure, P_{exp}, indicated as black circles in Fig. 7a. The oil intrusion pressure of the NFC membrane ranged from *ca.* 10 to over 30 kPa, with the value increasing with the increasing thickness of the electrospun CA layer.

The experimental oil intrusion pressure was then compared with the theoretical oil intrusion pressure, P_{theo}, which is indi-

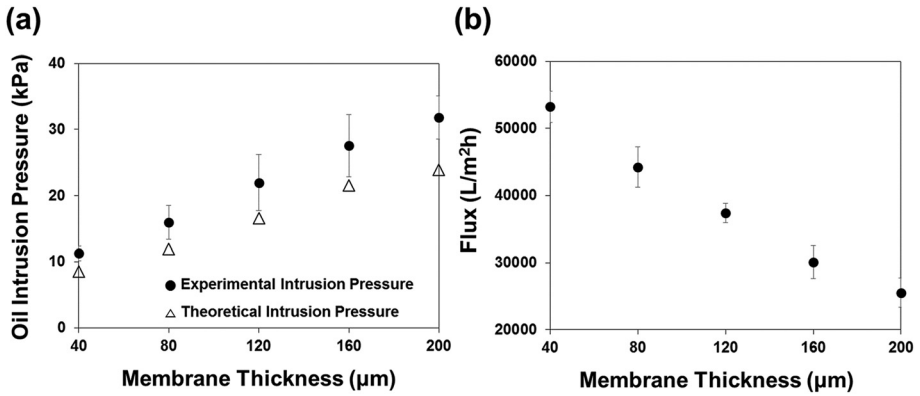

Fig. 7 (a) Oil intrusion pressure (for mineral oil) of the NFC membrane. (b) Oil/water separation flux of the NFC membrane as a function of membrane thickness.

cated as blank triangles in Fig. 7a. The theoretical oil intrusion pressure was calculated using eqn (2),

$$P_{\text{theo}} = 2\gamma_{L_1L_2}\cos\theta_0/d \quad (2)$$

where $\gamma_{L_1L_2}$ is the oil/water interfacial tension, θ_0 is the underwater OCA (mineral oil), and d is the effective pore diameter of the membrane. Porosimetry was used to obtain the pore size distribution and effective pore diameter of the NFC membranes. The largest pore diameter was used here, assuming that the oil droplet would have passed through the largest pore first upon the application of pressure. The largest pore diameters for the five NFC membranes and the corresponding theoretical oil intrusion pressures are presented in Table 1. Thicker membranes had smaller effective pore diameters, which led to larger theoretical oil intrusion pressures.

The trend of increasing oil intrusion pressure with the increasing membrane thickness was found for both the experimental and the theoretical cases. However, the theoretical oil intrusion pressure was smaller than the experimental value for all NFC membrane thicknesses. This discrepancy was caused by the limitation of being unable to capture the exact moment the oil droplet penetrated into the membrane when measuring the experimental oil intrusion pressure. The penetrated oil droplet took some time to travel all the way down to the other side of the membrane, at which point it was noticed, the time during which the applied pressure was constantly increasing. Therefore, the measured pressure was always greater than that at the exact moment when the membrane was penetrated. The discrepancy increased with increasing membrane thickness because it took a longer time for the oil droplet to travel through the membrane and be captured in the video. This is shown in the graph as a widening gap between the experimental value and the theoretical value with increasing membrane thickness.

Table 1 Largest pore diameters and the corresponding oil intrusion pressures for each NFC membrane with different thicknesses

Membrane thickness (μm)	Largest pore diameter (μm)	Theoretical oil intrusion pressure (kPa)
40	5.86	8.57
80	4.21	11.93
120	3.02	16.63
160	2.33	21.55
200	2.10	23.91

Fig. 7b shows how the oil/water separation flux changed with increasing NFC membrane thickness. The separation tests were carried out solely using gravity. The separation flux ranged from over 50 000 to 25 000 L m^{-2} h^{-1} as the thickness of the membrane increased from 40 to 200 μm.

3.7. Oil/water separation under the application of pressure

Previous studies on underwater superoleophobic membranes, which are capable of gravity-driven oil/water separation, did not explore the possibility of applying extra pressure for maximum separation flux during oil/water separation. This was mainly due to the oil intrusion pressure of previous membranes being relatively low; they would fail to keep the oil layer from penetrating even at low pressures. In contrast, by taking advantage of the NFC membrane's high oil intrusion pressure, the oil/water separation flux of the membrane could be drastically enhanced by deliberately applying pressure during the separation process. Fig. 8 shows the separation flux of the NFC membranes of different thicknesses as a function of applied pressure. The oil/water separation flux was measured at the various pressures indicated up to the oil intrusion pressure. The flux of each membrane increased with increasing applied pressure. The 200 μm-thick membrane had a flux that reached 120 000 L m^{-2} h^{-1} at 25 kPa, which is nearly six times greater than the original flux during gravity-driven oil/water separation. This result suggests that NFC membranes of appropriate thicknesses can facilitate large volumes of oil/water separations at high flux.

The increase in flux for each membrane diminished as the pressure approached its experimental oil intrusion pressure. This is in agreement with the previously noted observation

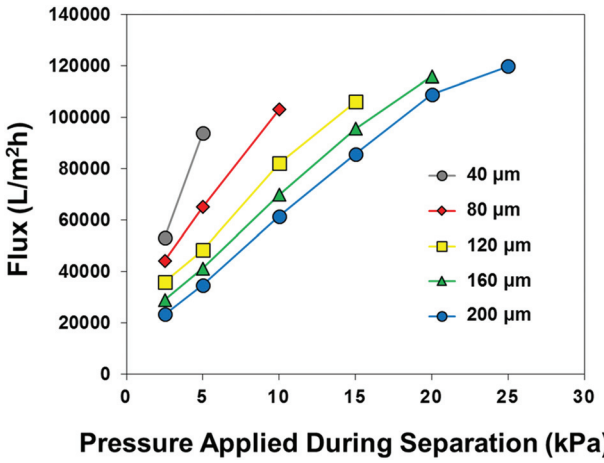

Fig. 8 Increase of separation flux for NFC membranes of different thicknesses as a function of the pressure applied during the oil/water separation.

that the experimental oil intrusion pressure was larger than the theoretical one, and was possibly approaching the actual oil intrusion pressure of the membrane. Each membrane was expected to be slightly penetrated by the oil layer when the applied pressure approached the experimental oil intrusion pressure, which caused the diminished flux gain with increasing pressure.

4. Conclusions

This research developed and studied the performance of an NFC membrane, which is a nanofibrous membrane capable of both gravity- and pressure-driven oil/water separation even in harsh environments such as strongly acidic, alkaline, or saline conditions. The NFC membrane displayed superb underwater superoleophobicity and successfully separated various types of oil/water mixtures at separation efficiencies exceeding 99%, driven only by gravity and also in chemically harsh environments. A single membrane could be used for repetitive oil/water separations, during which the oil content in the filtrate remained extremely low (<29 ppm). The membrane exhibited a high oil/water separation flux and high oil intrusion pressure. The enhanced oil intrusion pressure enabled pressure-driven oil/water separation, when the oil/water separation flux could reach 120 000 L m^{-2} h^{-1}. The superior durability of the NFC membrane against applied pressure and chemically harsh environments suggests that it could be effectively used in areas where large-scale oil/water separations with high flux are required.

Conflicts of interest

There are no conflicts to declare.

Acknowledgements

This work was supported by the National Research Foundation of Korea (NRF) grants funded by the Korean government (no. 2015R1A2A1A14027903, no. 011-0030075, and no. 2017R1E1A2A01077172).

References

1 J. Zhang and S. Seeger, *Adv. Funct. Mater.*, 2011, **21**, 4699–4704.
2 N. Liu, Y. Chen, F. Lu, Y. Cao, Z. Xue, K. Li, L. Feng and Y. Wei, *ChemPhysChem*, 2013, **14**, 3489–3494.
3 L. Zhang, Y. Zhong, D. Cha and P. Wang, *Sci. Rep.*, 2013, **3**, 2326.
4 W. Liang and Z. Guo, *RSC Adv.*, 2013, **3**, 16469.
5 B. Wang and Z. Guo, *Chem. Commun.*, 2013, **49**, 9416.
6 A. Li, H.-X. Sun, D.-Z. Tan, W.-J. Fan, S.-H. Wen, X.-J. Qing, G.-X. Li, S.-Y. Li and W.-Q. Deng, *Energy Environ. Sci.*, 2011, **4**, 2062.
7 S. J. Maguire-boyle and A. R. Barron, *J. Membr. Sci.*, 2011, **382**, 107–115.
8 C. R. Crick, J. A. Gibbins and I. P. Parkin, *J. Mater. Chem. A*, 2013, **1**, 5943.
9 S. J. Cho, H. Nam, H. Ryu and G. Lim, *Adv. Funct. Mater.*, 2013, **23**, 5577–5584.
10 C. Wang, T. Yao, J. Wu, C. Ma, Z. Fan, Z. Wang, Y. Cheng, Q. Lin and B. Yang, *ACS Appl. Mater. Interfaces*, 2009, **1**, 2613–2617.
11 J. Lin, B. Ding, J. Yang, J. Yu and G. Sun, *Nanoscale*, 2012, **4**, 176–182.
12 J. Wu, N. Wang, L. Wang, H. Dong, Y. Zhao and L. Jiang, *ACS Appl. Mater. Interfaces*, 2012, **4**, 3207–3212.
13 C. Gao, Z. Sun, K. Li, Y. Chen, Y. Cao, S. Zhang and L. Feng, *Energy Environ. Sci.*, 2013, **6**, 1147.
14 Q. Zhu and Q. Pan, *ACS Nano*, 2014, **8**, 1402–1409.
15 Y. Lu, S. Sathasivam, J. Song, F. Chen, W. Xu, C. J. Carmalt and I. P. Parkin, *J. Mater. Chem. A*, 2014, **2**, 11628–11634.
16 X. Zhou, Z. Zhang, X. Xu, F. Guo, X. Zhu, X. Men and B. Ge, *ACS Appl. Mater. Interfaces*, 2013, **5**, 7208–7214.
17 Q. An, Y. Zhang, K. Lv, X. Luan, Q. Zhang and F. Shi, *Nanoscale*, 2015, **7**, 4553–4558.
18 J. Song, S. Huang, Y. Lu, X. Bu, J. E. Mates, A. Ghosh, R. Ganguly, C. J. Carmalt, I. P. Parkin, W. Xu and C. M. Megaridis, *ACS Appl. Mater. Interfaces*, 2014, **6**(22), 19858–19865.
19 B. Cortese, D. Caschera, F. Federici, G. M. Ingo and G. Gigli, *J. Mater. Chem. A*, 2014, **2**, 6781–6789.
20 Y. Wang, S. Tao and Y. An, *J. Mater. Chem. A*, 2013, **1**, 1701–1708.
21 M. N. Kavalenka, A. Hopf, M. Schneider, M. Worgull and H. Hölscher, *RSC Adv.*, 2014, **4**, 31079–31083.
22 J. Li, H. M. Cheng, C. Y. Chan, P. F. Ng, L. Chen, B. Fei and J. H. Xin, *RSC Adv.*, 2015, **5**, 51537–51541.
23 M. Nosonovsky, *Nature*, 2011, **477**, 412–413.

24 Z. Xue, S. Wang, L. Lin, L. Chen, M. Liu, L. Feng and L. Jiang, *Adv. Mater.*, 2011, **23**, 4270–4273.
25 C. Teng, X. Lu, G. Ren, Y. Zhu, M. Wan and L. Jiang, *Adv. Mater. Interfaces*, 2014, 1–5.
26 H. C. Yang, J. K. Pi, K. J. Liao, H. Huang, Q. Y. Wu, X. J. Huang and Z. K. Xu, *ACS Appl. Mater. Interfaces*, 2014, **6**, 12566–12572.
27 J. Li, L. Yan, H. Li, W. Li, F. Zha and Z. Lei, *J. Mater. Chem. A*, 2015, **3**, 14696–14702.
28 L. Li, Z. Liu, Q. Zhang, C. Meng, T. Zhang and J. Zhai, *J. Mater. Chem. A*, 2015, **3**, 1279–1286.
29 M. A. Gondal, M. S. Sadullah, M. A. Dastageer, G. H. McKinley, D. Panchanathan and K. K. Varanasi, *ACS Appl. Mater. Interfaces*, 2014, **6**, 13422–13429.
30 D. Tian, X. Zhang, Y. Tian, Y. Wu, X. Wang, J. Zhai and L. Jiang, *J. Mater. Chem.*, 2012, **22**, 19652.
31 J. Li, L. Yan, W. Li, J. Li, F. Zha and Z. Lei, *Mater. Lett.*, 2015, **153**, 62–65.
32 P.-C. Chen and Z.-K. Xu, *Sci. Rep.*, 2013, **3**, 4487–4492.
33 F. Zhang, W. Bin Zhang, Z. Shi, D. Wang, J. Jin and L. Jiang, *Adv. Mater.*, 2013, **25**, 4192–4198.
34 Z. Cheng, H. Lai, Y. Du, K. Fu, R. Hou, C. Li, N. Zhang and K. Sun, *ACS Appl. Mater. Interfaces*, 2014, **6**(1), 636–641.
35 Q. Wen, J. Di, L. Jiang, J. Yu and R. Xu, *Chem. Sci.*, 2013, **4**, 591–595.
36 Y. Dong, J. Li, L. Shi, X. Wang, Z. Guo and W. Liu, *Chem. Commun.*, 2014, **50**, 5586.
37 Y. Huang, H. Li, L. Wang, Y. Qiao, C. Tang, C. Jung, Y. Yoon, S. Li and M. Yu, *Adv. Mater. Interfaces*, 2015, **2**, 1–7.
38 J. Li, D. Li, Y. Yang, J. Li, F. Zha and Z. Lei, *Green Chem.*, 2016, 541–549.
39 L. Liu, C. Chen, S. Yang, H. Xie, M. Gong and X. Xu, *Phys. Chem. Chem. Phys.*, 2016, **18**, 1317–1325.
40 C. Clark and J. Veil, *Argonne Natl. Lab., Rep.*, 2009, 64.